

# Lecture 19

## More on Hollow Waveguides

We have seen that the hollow waveguide is the simplest of waveguides. Closed form solutions exist for such waveguides as seen in the rectangular waveguide case. The solution is elegantly simple and beautiful requiring only trigonometric functions. So we will continue with the study of the rectangular waveguide, and then address another waveguide, the circular waveguide where closed form solutions exist also. However, the solution has to be expressed in terms of “Bessel functions”, called special functions. As the name implies, these functions are seldom used outside the context of studying wave phenomena. Bessel functions in cylindrical coordinates are the close cousin of the sinusoidal functions in cartesian coordinates. Whether Bessel functions are more complex or esoteric compared to sinusoidal functions is in the eye of the beholder. Once one is familiarized with them, they are simple. They are also the function that describes the concentric ripple wave that you see in your tea cup every morning (see Figure 19.1)!



Figure 19.1: The ripple wave in your tea cup is describable by a Bessel function (courtesy of dreamstime.com).

## 19.1 Rectangular Waveguides, Contd.

We have seen the mathematics for the TE modes of a rectangular waveguide. We shall study the TM modes and the modes of a circular waveguide in this lecture.

### 19.1.1 TM Modes ( $E_z \neq 0$ , E Modes or $\text{TM}_z$ Modes)

These modes are not the exact dual of the TE modes because of the boundary conditions. The dual of a PEC (perfect electric conducting) wall is a PMC (perfect magnetic conducting) wall. However, the previous exercise for TE modes can be repeated for the TM modes with caution on the boundary conditions. The scalar wave function (or eigenfunction/eigenmode) for the TM modes, satisfying the homogeneous Dirichlet (instead of Neumann)<sup>1</sup> boundary condition with  $(\Psi_{es}(\mathbf{r}_s) = 0)$  on the entire waveguide wall is

$$\Psi_{es}(x, y) = A \sin\left(\frac{m\pi}{a}x\right) \sin\left(\frac{n\pi}{b}y\right) \quad (19.1.1)$$

Here, sine functions are chosen for the standing waves, and the chosen values of  $\beta_x$  and  $\beta_y$  ensure that the boundary condition is satisfied on the  $x = a$  and  $y = b$  walls. Neither of the  $m$  and  $n$  can be zero, lest  $\Psi_{es}(x, y) = 0$ , or the field is zero. Hence, both  $m > 0$ , and  $n > 0$  are needed. Thus, the lowest TM mode is the  $\text{TM}_{11}$  mode. Thinking of this as an eigenvalue problem, then the eigenvalue is

$$\beta_s^2 = \beta_x^2 + \beta_y^2 = \left(\frac{m\pi}{a}\right)^2 + \left(\frac{n\pi}{b}\right)^2 \quad (19.1.2)$$

which is the same as the TE case. Therefore, the corresponding cutoff frequencies and cutoff wavelengths for the  $\text{TM}_{mn}$  modes are the same as the  $\text{TE}_{mn}$  modes. Also, these TE and TM modes are degenerate when they share the same eigenvalues. Furthermore, the lowest modes,  $\text{TE}_{11}$  and  $\text{TM}_{11}$  modes have the same cutoff frequency. Figure 19.2 shows the dispersion curves for different modes of a rectangular waveguide. Notice that the group velocities of all the modes are zero at cutoff, and then the group velocities approach that of the waveguide medium as frequency becomes large. These observations can be explained physically.

---

<sup>1</sup>Again, “homogeneous” here means “zero”.

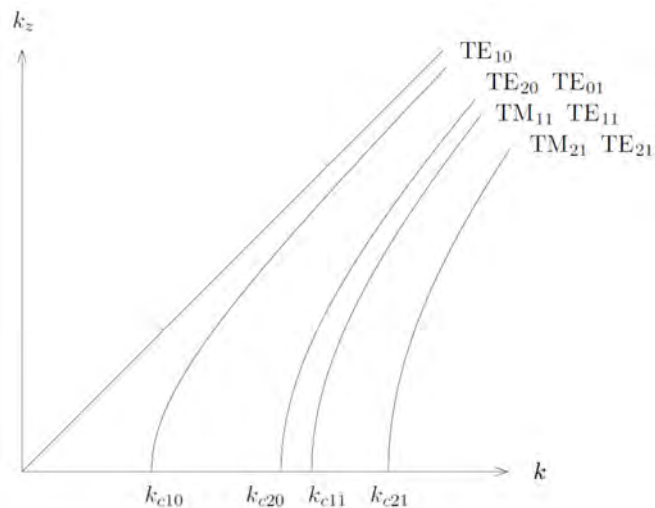


Figure 19.2: Dispersion curves for a rectangular waveguide (courtesy of J.A. Kong [32]). Notice that the lowest TM mode is the  $TM_{11}$  mode, and  $k$  is equivalent to  $\beta$  in this course. At cutoff, the guided mode does not propagate in the  $z$  direction, and here, the group velocity is zero. But when  $\omega \rightarrow \infty$ , the mode propagates in direction almost parallel to the axis of the waveguide, and hence, the group velocity approaches that of the waveguide medium.

### 19.1.2 Bouncing Wave Picture

We have seen that the transverse variation of a mode in a rectangular waveguide can be expanded in terms of sine and cosine functions which represent standing waves which are superposition of two traveling waves, or that they are

$$[\exp(-j\beta_x x) \pm \exp(j\beta_x x)] [\exp(-j\beta_y y) \pm \exp(j\beta_y y)]$$

When the above is expanded and together with the  $\exp(-j\beta_z z)$  the mode propagating in the  $z$  direction in addition to the standing waves in the transverse direction. Or we see four waves bouncing around in the  $xy$  directions and propagating in the  $z$  direction. The picture of this bouncing wave can be depicted in Figure 19.3.

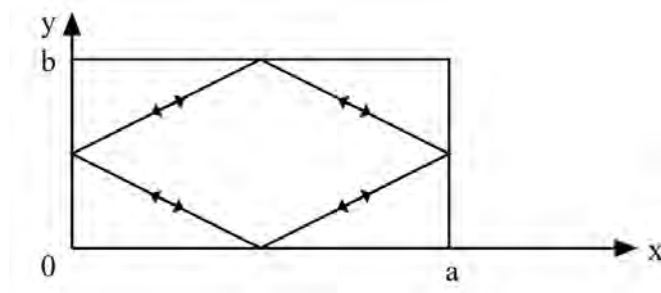


Figure 19.3: The waves in a rectangular waveguide can be thought of as bouncing waves off the four walls as they propagate in the  $z$  direction.

### 19.1.3 Field Plots

Given the knowledge of the scalar piloting potential of a waveguide, one can derive all the field components. For example, for the TE modes, if we know  $\Psi_h(\mathbf{r})$ , then

$$\mathbf{E} = \nabla \times \hat{z}\Psi_h(\mathbf{r}), \quad \mathbf{H} = -\nabla \times \mathbf{E}/(j\omega\mu) \quad (19.1.3)$$

Then all the electromagnetic field of a waveguide mode can be found, and similarly for TM modes.

Plots of the fields of different rectangular waveguide modes are shown in Figure 19.4. Notice that for higher  $m$ 's and  $n$ 's, with  $\beta_x = m\pi/a$  and  $\beta_y = n\pi/b$ , the corresponding  $\beta_x$  and  $\beta_y$  are larger with higher spatial frequencies. Thus, the transverse spatial wavelengths are getting shorter. Also, since  $\beta_z = \sqrt{\beta^2 - \beta_x^2 - \beta_y^2}$ , higher frequencies are needed to make  $\beta_z$  real in order to propagate the higher order modes or the high  $m$  and  $n$  modes.

Notice also how the electric field and magnetic field curl around each other. Since  $\nabla \times \mathbf{H} = j\omega\varepsilon\mathbf{E}$  and  $\nabla \times \mathbf{E} = -j\omega\mu\mathbf{H}$ , they do not curl around each other “immediately” but with a  $\pi/2$  phase delay due to the  $j\omega$  factor. Therefore, the  $\mathbf{E}$  and  $\mathbf{H}$  fields do not curl around each other at one location, but at a displaced location due to the  $\pi/2$  phase difference. This is shown in Figure 19.5.

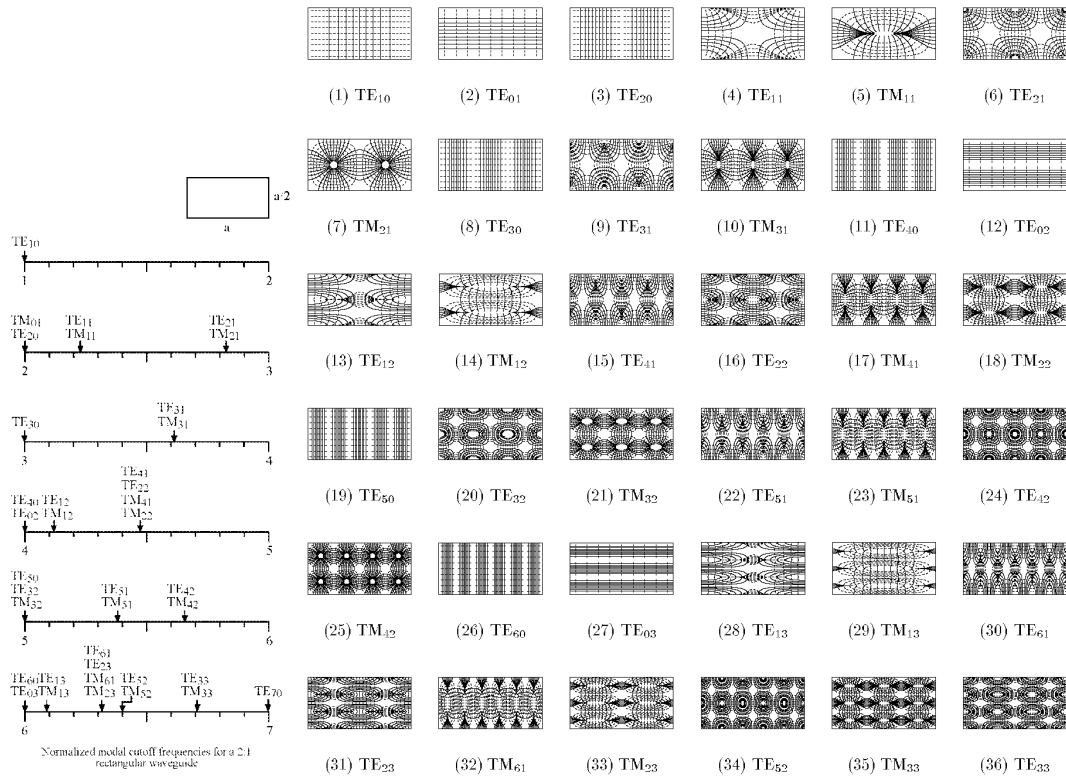


Figure 19.4: Transverse field plots of different modes in a rectangular waveguide (courtesy of Andy Greenwood. Original plots published in Lee, Lee, and Chuang, IEEE T-MTT, 33.3 (1985): pp. 271-274. [115]).

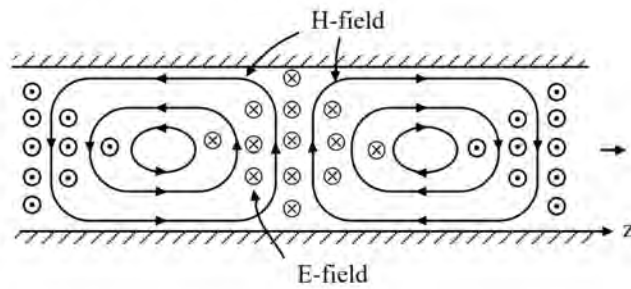


Figure 19.5: Field plot of a mode propagating in the  $z$  direction of a rectangular waveguide. Notice that the E and H fields do not exactly curl around each other.

## 19.2 Circular Waveguides

Another waveguide where closed-form solutions can be easily obtained is the circular hollow waveguide as shown in Figure 19.6, but they involve the use of Bessel functions.

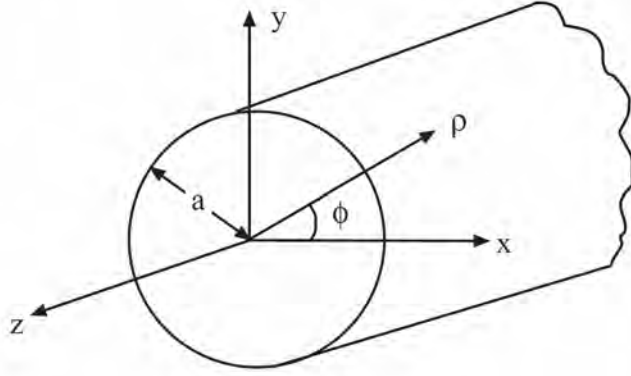


Figure 19.6: Schematic of a circular waveguide in cylindrical coordinates. It is one of the separable coordinate systems.

### 19.2.1 TE Case

For a circular waveguide, it is best first to express the Laplacian operator,  $\nabla_s^2 = \nabla_s \cdot \nabla_s$ , in cylindrical coordinates. The first  $\nabla_s$  is a gradient operator while the second  $\nabla_s \cdot$  is a divergence operator: they have different physical meanings. Formulas for grad and div operators are given in many text books [32, 116]. Doing a table lookup,

$$\nabla_s \Psi = \hat{\rho} \frac{\partial}{\partial \rho} \Psi + \hat{\phi} \frac{1}{\rho} \frac{\partial}{\partial \phi} \Psi$$

$$\nabla_s \cdot \mathbf{A} = \frac{1}{\rho} \frac{\partial}{\partial \rho} \rho A_\rho + \frac{1}{\rho} \frac{\partial}{\partial \phi} A_\phi$$

Then

$$(\nabla_s^2 + \beta_s^2) \Psi_{hs} = \left( \frac{1}{\rho} \frac{\partial}{\partial \rho} \rho \frac{\partial}{\partial \rho} + \frac{1}{\rho^2} \frac{\partial^2}{\partial \phi^2} + \beta_s^2 \right) \Psi_{hs}(\rho, \phi) = 0 \quad (19.2.1)$$

The above is the partial differential equation for field in a circular waveguide. It is an eigenvalue problem where  $\beta_s^2$  is the eigenvalue, and  $\Psi_{hs}(\mathbf{r}_s)$  is the eigenfunction (equivalence of an eigenvector). Using separation of variables, we let

$$\Psi_{hs}(\rho, \phi) = B_n(\beta_s \rho) e^{\pm jn\phi} \quad (19.2.2)$$

Then  $\frac{\partial^2}{\partial \phi^2} \rightarrow -n^2$ , and (19.2.1) simplifies to an ordinary differential equation which is

$$\left( \frac{1}{\rho} \frac{d}{d\rho} \rho \frac{d}{d\rho} - \frac{n^2}{\rho^2} + \beta_s^2 \right) B_n(\beta_s \rho) = 0 \quad (19.2.3)$$

Here, dividing the above equation by  $\beta_s^2$ , we can let  $\beta_s \rho$  in (19.2.2) and (19.2.3) be  $x$ . Then the above can be rewritten as

$$\left( \frac{1}{x} \frac{d}{dx} x \frac{d}{dx} - \frac{n^2}{x^2} + 1 \right) B_n(x) = 0 \quad (19.2.4)$$

The above is known as the Bessel equation whose solutions are special functions denoted as  $B_n(x)$ .<sup>2</sup>

These special functions are  $J_n(x)$ ,  $N_n(x)$ ,  $H_n^{(1)}(x)$ , and  $H_n^{(2)}(x)$  which are called Bessel, Neumann, Hankel function of the first kind, and Hankel function of the second kind, respectively, where  $n$  is the order, and  $x$  is the argument.<sup>3</sup> Since this is a second order ordinary differential equation, it has only two independent solutions. Therefore, two of the four commonly encountered solutions of Bessel equation are independent. Thus, they can be expressed in terms of each other. Their relationships are shown below:<sup>4</sup>

$$\text{Bessel,} \quad J_n(x) = \frac{1}{2} [H_n^{(1)}(x) + H_n^{(2)}(x)] \quad (19.2.5)$$

$$\text{Neumann,} \quad N_n(x) = \frac{1}{2j} [H_n^{(1)}(x) - H_n^{(2)}(x)] \quad (19.2.6)$$

$$\text{Hankel-First kind,} \quad H_n^{(1)}(x) = J_n(x) + jN_n(x) \quad (19.2.7)$$

$$\text{Hankel-Second kind,} \quad H_n^{(2)}(x) = J_n(x) - jN_n(x) \quad (19.2.8)$$

It can be shown that

$$H_n^{(1)}(x) \sim \sqrt{\frac{2}{\pi x}} e^{jx - j(n+\frac{1}{2})\frac{\pi}{2}}, \quad x \rightarrow \infty \quad (19.2.9)$$

$$H_n^{(2)}(x) \sim \sqrt{\frac{2}{\pi x}} e^{-jx + j(n+\frac{1}{2})\frac{\pi}{2}}, \quad x \rightarrow \infty \quad (19.2.10)$$

They correspond to traveling wave solutions when  $x = \beta_s \rho \rightarrow \infty$ . Since  $J_n(x)$  and  $N_n(x)$  are linear superpositions of these traveling wave solutions, they correspond to standing wave solutions. Moreover,  $N_n(x)$ ,  $H_n^{(1)}(x)$ , and  $H_n^{(2)}(x) \rightarrow \infty$  when  $x \rightarrow 0$ . Since the field has to be regular when  $\rho \rightarrow 0$  at the center of the waveguide shown in Figure 19.6, the only viable solution for the hollow waveguide, to be chosen from (19.2.5) to (19.2.9), is that  $B_n(\beta_s \rho) = AJ_n(\beta_s \rho)$ . Thus for a circular hollow waveguide, the eigenfunction or mode is of the form

$$\Psi_{hs}(\rho, \phi) = AJ_n(\beta_s \rho) e^{\pm jn\phi} \quad (19.2.11)$$

<sup>2</sup>Studied by Friedrich Wilhelm Bessel, 1784-1846.

<sup>3</sup>Some textbooks use  $Y_n(x)$  for Neumann functions.

<sup>4</sup>Their relations with each other are similar to those between  $\exp(-jx)$ ,  $\sin(x)$ , and  $\cos(x)$ .

To ensure that the eigenfunction and the eigenvalue are unique, boundary condition for the partial differential equation is needed. The homogeneous Neumann boundary condition,<sup>5</sup> or that  $\partial_n \Psi_{hs} = 0$ , on the PEC waveguide wall then translates to

$$\frac{d}{d\rho} J_n(\beta_s \rho) = 0, \quad \rho = a \quad (19.2.12)$$

Defining  $J_n'(x) = \frac{d}{dx} J_n(x)$ ,<sup>6</sup> the above is the same as

$$J_n'(\beta_s a) = 0 \quad (19.2.13)$$

The above are the zeros of the derivative of Bessel function and they are tabulated in many textbooks and handbooks. The  $m$ -th zero of  $J_n'(x)$  is denoted to be  $\beta_{nm}$  in many books.<sup>7</sup> Plots of Bessel functions and their derivatives are shown in Figure 19.8, and some zeros of Bessel function and its derivative are also shown in Figure 19.9. With this knowledge, the guidance condition for a waveguide mode is then

$$\beta_s = \beta_{nm}/a \quad (19.2.14)$$

for the  $\text{TE}_{nm}$  mode. From the above,  $\beta_s^2$  can be obtained which is the eigenvalue of (19.2.1) and (19.2.3). It is a constant independent of frequency.

Using the fact that  $\beta_z = \sqrt{\beta^2 - \beta_s^2}$ , then  $\beta_z$  will become pure imaginary if  $\beta^2$  is small enough (or the frequency low enough) so that  $\beta^2 < \beta_s^2$  or  $\beta < \beta_s$ . From this, the corresponding cutoff frequency (the frequency below which  $\beta_z$  becomes pure imaginary) of the  $\text{TE}_{nm}$  mode is

$$\omega_{nm,c} = \frac{1}{\sqrt{\mu\varepsilon}} \frac{\beta_{nm}}{a} \quad (19.2.15)$$

When  $\omega < \omega_{nm,c}$ , the corresponding mode cannot propagate in the waveguide as  $\beta_z$  becomes pure imaginary. The corresponding cutoff wavelength is

$$\lambda_{nm,c} = \frac{2\pi}{\beta_{nm}} a \quad (19.2.16)$$

By the same token, when  $\lambda > \lambda_{nm,c}$ , the corresponding mode cannot be guided by the waveguide. It is not exactly precise to say this, but this gives us the heuristic notion that if wavelength or “size” of the wave or photon is too big, it cannot fit inside the waveguide.

## 19.2.2 TM Case

The corresponding partial differential equation and boundary value problem for this case is

$$\left( \frac{1}{\rho} \frac{\partial}{\partial \rho} \rho \frac{\partial}{\partial \rho} + \frac{1}{\rho^2} \frac{\partial^2}{\partial \phi^2} + \beta_s^2 \right) \Psi_{es}(\rho, \phi) = 0 \quad (19.2.17)$$

<sup>5</sup>Note that “homogeneous” here means “zero” in math.

<sup>6</sup>Note that this is a standard math notation, which has a different meaning in some engineering texts.

<sup>7</sup>Notably, Abramowitz and Stegun, Handbook of Mathematical Functions [117]. An online version is available at [118].



with the homogeneous Dirichlet boundary condition,  $\Psi_{es}(a, \phi) = 0$ , on the waveguide wall. The eigenfunction solution is

$$\Psi_{es}(\rho, \phi) = AJ_n(\beta_s \rho)e^{\pm jn\phi} \tag{19.2.18}$$

with the boundary condition that  $J_n(\beta_s a) = 0$ . The zeros of  $J_n(x)$  are labeled as  $\alpha_{nm}$  in many textbooks, as well as in Figure 19.9; and hence, the guidance condition is that for the  $TM_{nm}$  mode is that

$$\beta_s = \frac{\alpha_{nm}}{a} \tag{19.2.19}$$

where the eigenvalue for (19.2.17) is  $\beta_s^2$  which is a constant independent of frequency. With  $\beta_z = \sqrt{\beta^2 - \beta_s^2}$ , the corresponding cutoff frequency is

$$\omega_{nm,c} = \frac{1}{\sqrt{\mu\varepsilon}} \frac{\alpha_{nm}}{a} \tag{19.2.20}$$

or when  $\omega < \omega_{nm,c}$ , the mode cannot be guided. The cutoff wavelength is

$$\lambda_{nm,c} = \frac{2\pi}{\alpha_{nm}} a \tag{19.2.21}$$

with the notion that when  $\lambda > \lambda_{nm,c}$ , the mode cannot be guided.

It turns out that the lowest mode in a circular waveguide is the  $TE_{11}$  mode. It is actually a close cousin of the  $TE_{10}$  mode of a rectangular waveguide. This can be gathered by comparing their field plots: these modes morph into each other as we deform the shape of a rectangular waveguide into a circular waveguide.

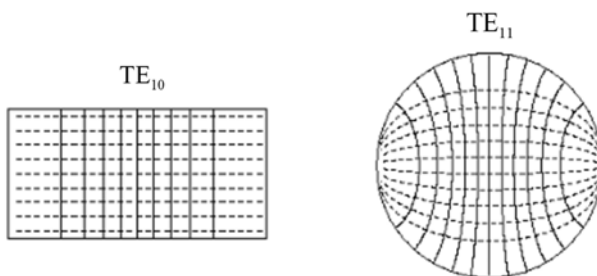


Figure 19.7: Side-by-side comparison of the field plots of the  $TE_{10}$  mode of a rectangular waveguide versus that of the  $TE_{11}$  mode of a circular waveguide. If one is imaginative enough, one can see that the field plot of one mode morphs into that of the other mode. Electric fields are those that have to end on the waveguide walls.

Figure 19.8 shows the plots of Bessel function  $J_n(x)$  and its derivative  $J'_n(x)$ . Tables in Figure 19.9 show the roots of  $J'_n(x)$  and  $J_n(x)$  which are important for determining the cutoff frequencies of the TE and TM modes of circular waveguides.

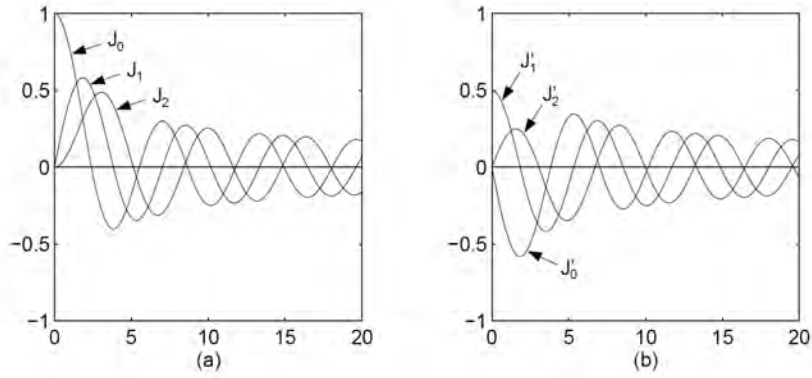


Figure 19.8: Plots of the Bessel function,  $J_n(x)$ , and its derivatives  $J'_n(x)$ . The zeros of these functions are used to find the eigenvalue  $\beta_s^2$  of the problem, and hence, the guidance condition. The left figure is for TM modes, while the right figure is for TE modes. Here,  $J'_n(x) = dJ_n(x)/dx$ .

Table 2.3.1. Roots of  $J'_n(x) = 0$ .

n	$\beta_{n1}$	$\beta_{n2}$	$\beta_{n3}$	$\beta_{n4}$
0	3.832	7.016	10.174	13.324
1	1.841	5.331	8.536	11.706
2	3.054	6.706	9.970	13.170
3	4.201	8.015	11.346	14.586
4	5.318	9.282	12.682	15.964
5	6.416	10.520	13.987	17.313

Table 2.3.2. Roots of  $J_n(x) = 0$ .

n	$\alpha_{n1}$	$\alpha_{n2}$	$\alpha_{n3}$	$\alpha_{n4}$
0	2.405	5.520	8.654	11.792
1	3.832	7.016	10.174	13.324
2	5.135	8.417	11.620	14.796
3	6.380	9.761	13.015	16.223
4	7.588	11.065	14.373	17.616
5	8.771	12.339	15.700	18.980

Figure 19.9: Table 2.3.1 shows the zeros of  $J'_n(x)$ , which are useful for determining the guidance conditions of the  $TE_{mn}$  mode of a circular waveguide. On the other hand, Table 2.3.2 shows the zeros of  $J_n(x)$ , which are useful for determining the guidance conditions of the  $TM_{mn}$  mode of a circular waveguide.

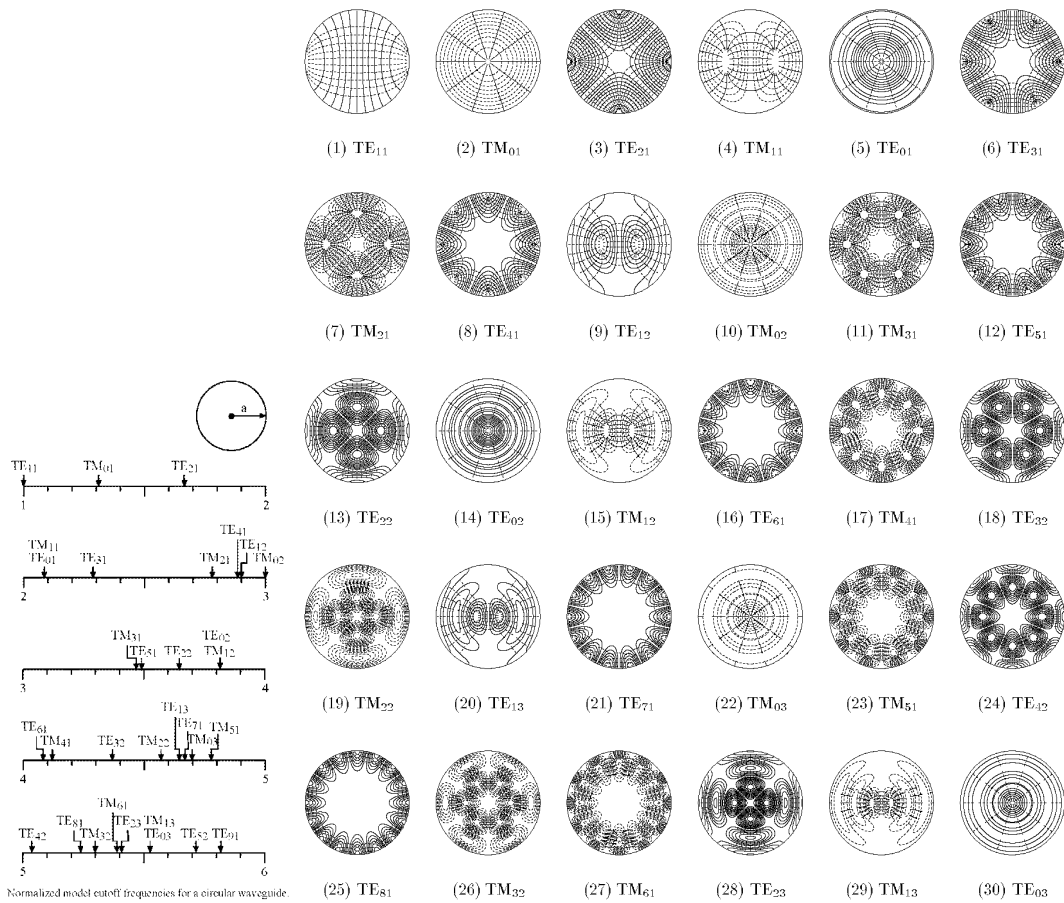


Figure 19.10: Transverse field plots of different modes in a circular waveguide (courtesy of Andy Greenwood. Original plots published in Lee, Lee, and Chuang [115]). The axially symmetric TE<sub>01</sub> mode has the lowest loss, and finds a number of real-world applications as in radio astronomy.

